IRSTI 29.19.22 https://doi.org/10.26577/ijmph.2023.v14.i1.010

Ç. Allahverdi

Toros University, Mersin, Turkey
e-mail: cagdas.allahverdi@toros.edu.tr
(Received 23 February 2023; accepted 17 April 2023)

Slow growth of CdSe nanocrystals in glass and their refractive index change

Abstract. The refractive index change of semiconductor nanocrystals must be known when designing precision optical components based on semiconductor nanocrystals. In this study, Kramers-Kronig transformation has been used to compute the linear refractive index change of cadmium selenide (CdSe) nanocrystals embedded in glass. Classical theory and numerical computation of Kramers-Kronig relation have been given and explained in detail. CdSe nanocrystals have been grown in borosilicate glass by using melting, rapid-cooling, and heat treatment procedure. Compared to the production studies of semiconductor nanocrystals in borosilicate glass in the literature, the growth temperature of CdSe nanocrystals in glass has been decreased and their growth time has been extended. In other words, a slow growth method has been performed to form pure CdSe nanocrystals in glass. The quantum size effect has been observed at their optical absorption spectra. Surface and longitudinal optical phonon modes of CdSe nanocrystals have been measured by using Raman spectroscopy. The refractive index change has been found as ~1.36×10^{-4} for CdSe nanocrystals with a diameter of ~3.93 nm.
Key words: CdSe, nanocrystal, glass, BaF_2, refractive index change, Kramers-Kronig.

Introduction

Kramers-Kronig transformation is taken its name from physicists Hendrik Anthony Kramers and Ralph Kronig. Kramers and Kronig obtained these relations independently in 1926 and 1927 [1, 2]. Kramers-Kronig (K-K) transformations can be stated as in Eq. 1 or Eq. 2.

$$\chi_1(\omega) = \frac{1}{\pi} P \int_{-\infty}^{\infty} \frac{\chi_2(\Omega)}{\Omega-\omega} d\Omega \qquad (1)$$

$$\chi_2(\omega) = -\frac{1}{\pi} P \int_{-\infty}^{\infty} \frac{\chi_1(\Omega)}{\Omega-\omega} d\Omega \qquad (2)$$

Here, $\chi_1(\omega)$ and $\chi_2(\omega)$ are angular frequency dependent real and imaginary parts of susceptibility (χ), respectively. As can be understood from Eq. 1 and Eq. 2, K-K relations enable us to obtain real part of a complex physical quantity from its imaginary part and vice versa. Refractive index, dielectric constant, and shear modulus are examples of complex physical quantities. K-K relations have been used to extract real or imaginary parts of such complex physical quantities [3, 4]. K-K relations are based on the principle of causality [5]. According to the causality principle, a cause comes before its effect. For example, first light photons enter the optical material and encounter with a scattering center, and then scattering occurs. Light scattering cannot be happened without a scattering center.

In this paper, CdSe nanocrystals have been nucleated and grown in glass by melting, rapid cooling, and heat treatment procedure. Lower temperature and prolonged time at heat treatment stage when compared with the studies in literature have been used to produce small and pure CdSe nanocrystals in borosilicate glass [6-8]. Composition of CdSe nanocrystals has been determined by Raman spectroscopy. Optical absorption coefficient of CdSe nanocrystals in glass has been measured. In the literature, linear refractive index change of CdSe nanocrystals in glass has not been studied. Therefore, linear refractive index change of CdSe nanocrystals in glass has been computed by K-K transformation. Trapezoidal method (a numerical summation

method) has been used to compute real part of refractive index from the absorption coefficient of CdSe nanocrystals in glass. This numerical computing approach explained here can also be applied to a variety of materials such as transparent liquids, solutions of food coloring dyes, and nanocrystals dispersed in solution.

Refractive Index Change of Chalcogenide Semiconductor Nanocrystals

Moreels et al. investigated complex dielectric function of colloidal lead sulfide (PbS), lead selenide (PbSe) and lead telluride (PbTe) nanocrystals (also known as quantum dots) by K-K analysis. Absorption coefficient of the nanocrystals was obtained using Maxwell-Garnett effective medium theory. Real and imaginary parts of the dielectric function of these nanocrystals whose average diameters are between 3.0-10.0 nm were determined in the wavelength range of 0-2500 nm [9]. Refractive index of PbS nanocrystals in glass was also calculated by Moreels et al. PbS nanocrystals increased refractive index of glass about 2.5-3.5×10^{-3} between 400-1800 nm when PbS nanocrystals having 4.4 nm diameter were growth in glass at a volume fraction of 0.146% [10]. Complex refractive indices of films of CdSe and CdS capped CdSe nanocrystals were measured between 400-800 nm by Dement et al. They showed that K-K iterative procedure produced close results to that of spectroscopic ellipsometry [11]. Refractive index change of ZnS capped CdSe nanocrystals adsorbed on bimetallic film coated glass fiber was investigated by Nguyen et al. [12]. K-K relations were also utilized to calculate nonlinear refractive index of semiconductor nanocrystals [13, 14].

Theory of K-K Transformation

In this section, primarily derivation of Eq. 1 and Eq. 2 will be given in detail. According to the Cauchy's residue theorem, closed integral of $\chi(\Omega)/(\Omega-\omega)$ is zero over the contour C shown in Fig. 1.

Thus, Eq. 3 is written.

$$\oint_C \frac{\chi(\Omega)}{\Omega-\omega} d\Omega = 0 \tag{3}$$

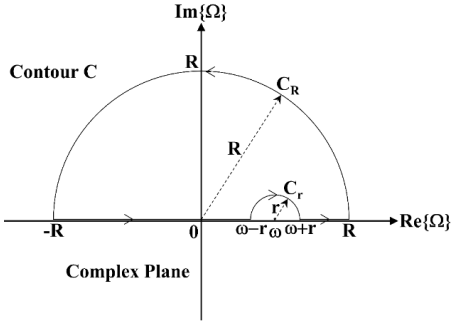

Figure 1 – Closed C curve at complex plane.
R and r are radii of curves of C_R and C_r, respectively.

This closed integral in Eq. 3 is separated to 4 integrals.

$$\oint_C \frac{\chi(\Omega)}{\Omega-\omega} d\Omega = \int_{-R}^{\omega-r} \frac{\chi(\Omega)}{\Omega-\omega} d\Omega + \int_{C_r} \frac{\chi(\Omega)}{\Omega-\omega} d\Omega + \int_{\omega+r}^{R} \frac{\chi(\Omega)}{\Omega-\omega} d\Omega + \int_{C_R} \frac{\chi(\Omega)}{\Omega-\omega} d\Omega = 0 \tag{4}$$

If radius r goes to 0 (sufficiently small) and radius R goes to ∞ (sufficiently large), Eq. 4 is written as follows.

$$\lim_{R\to\infty} \lim_{r\to 0} \left[\int_{-R}^{\omega-r} \frac{\chi(\Omega)}{\Omega-\omega} d\Omega + \int_{C_r} \frac{\chi(\Omega)}{\Omega-\omega} d\Omega + \int_{\omega+r}^{R} \frac{\chi(\Omega)}{\Omega-\omega} d\Omega + \int_{C_R} \frac{\chi(\Omega)}{\Omega-\omega} d\Omega \right] = 0 \tag{5}$$

$$\lim_{R\to\infty} \left[\int_{-R}^{\omega} \frac{\chi(\Omega)}{\Omega-\omega} d\Omega + \lim_{r\to 0} \int_{C_r} \frac{\chi(\Omega)}{\Omega-\omega} d\Omega + \int_{\omega}^{R} \frac{\chi(\Omega)}{\Omega-\omega} d\Omega + \int_{C_R} \frac{\chi(\Omega)}{\Omega-\omega} d\Omega \right] = 0 \tag{6}$$

In Eq. 6, the integral over C_r is solved by using substitution. This substitution is given at Eq. 7.

$$\Omega = \omega + re^{i\theta} \tag{7}$$

$$d\Omega = re^{i\theta} i d\theta \tag{8}$$

Eq. 7 depicts C_r curve in the complex-plane (see Fig. 1). r and θ are polar coordinates. Differential form of Eq. 7 is Eq. 8. If Eq. 7 and Eq. 8 are used, the integral over C_r becomes as follows.

$$\lim_{r\to 0} \int_{C_r} \frac{\chi(\Omega)}{\Omega-\omega} d\Omega = \lim_{r\to 0} \int_{\pi}^{0} \frac{\chi(\omega+re^{i\theta})}{\omega+re^{i\theta}-\omega} re^{i\theta} i d\theta = -i\pi\chi(\omega) \tag{9}$$

If Eq. 9 is used in Eq. 6, Eq. 6 will be

$$\lim_{R\to\infty}\left[\int_{-R}^{\omega}\frac{\chi(\Omega)}{\Omega-\omega}d\Omega-i\pi\chi(\omega)+\int_{\omega}^{R}\frac{\chi(\Omega)}{\Omega-\omega}d\Omega+\int_{C_R}\frac{\chi(\Omega)}{\Omega-\omega}d\Omega\right]=0 \quad (10)$$

$$\lim_{R\to\infty}\left[\int_{-R}^{\omega}\frac{\chi(\Omega)}{\Omega-\omega}d\Omega+\int_{\omega}^{R}\frac{\chi(\Omega)}{\Omega-\omega}d\Omega\right]-i\pi\chi(\omega)+\lim_{R\to\infty}\int_{C_R}\frac{\chi(\Omega)}{\Omega-\omega}d\Omega=0 \quad (11)$$

When R goes to ∞, the integral over C_R will equal to 0 in accordance with Jordan's lemma [15]. Therefore, Eq. 11 is given as follows.

$$\lim_{R\to\infty}\int_{-R}^{R}\frac{\chi(\Omega)}{\Omega-\omega}d\Omega-i\pi\chi(\omega)+0=0 \quad (12)$$

$$P\int_{-\infty}^{\infty}\frac{\chi(\Omega)}{\Omega-\omega}d\Omega-i\pi\chi(\omega)=0 \quad (13)$$

$$\chi(\omega)=\frac{1}{i\pi}P\int_{-\infty}^{\infty}\frac{\chi(\Omega)}{\Omega-\omega}d\Omega \quad (14)$$

Eq. 14 is K-K relation. In Eq. 14, P indicates Cauchy principal value. In Eq. 14, if $\Omega=\omega$, singularity is avoided by the Cauchy principal value. As mentioned above, susceptibility consists of real and imaginary parts and so it is written as below.

$$\chi(\omega)=\chi_1(\omega)+i\chi_2(\omega) \quad (15)$$

$$\chi(\Omega)=\chi_1(\Omega)+i\chi_2(\Omega) \quad (16)$$

If $\chi(\omega)$ and $\chi(\Omega)$ in Eq. 14 are substituted by Eq. 15 and Eq. 16, respectively, Eq. 14 will be

$$\chi_1(\omega)+i\chi_2(\omega)=\frac{1}{i\pi}P\int_{-\infty}^{\infty}\frac{\chi_1(\Omega)+i\chi_2(\Omega)}{\Omega-\omega}d\Omega \quad (17)$$

$$\chi_1(\omega)+i\chi_2(\omega)=$$
$$=\frac{1}{i\pi}P\int_{-\infty}^{\infty}\frac{\chi_1(\Omega)}{\Omega-\omega}d\Omega+\frac{1}{\pi}P\int_{-\infty}^{\infty}\frac{\chi_2(\Omega)}{\Omega-\omega}d\Omega \quad (18)$$

$$\chi_1(\omega)+i\chi_2(\omega)=$$
$$=\frac{1}{\pi}P\int_{-\infty}^{\infty}\frac{\chi_2(\Omega)}{\Omega-\omega}d\Omega+i\frac{-1}{\pi}P\int_{-\infty}^{\infty}\frac{\chi_1(\Omega)}{\Omega-\omega}d\Omega \quad (19)$$

From Eq. 19, $\chi_1(\omega)$ and $\chi_2(\omega)$ are written as

$$\chi_1(\omega)=\frac{1}{\pi}P\int_{-\infty}^{\infty}\frac{\chi_2(\Omega)}{\Omega-\omega}d\Omega \quad (20)$$

$$\chi_2(\omega)=-\frac{1}{\pi}P\int_{-\infty}^{\infty}\frac{\chi_1(\Omega)}{\Omega-\omega}d\Omega \quad (21)$$

Thus, K-K transformations shown in Eq. 1 and Eq. 2 are obtained. By multiplying numerator and denominator of the integrand with $\Omega+\omega$ in Eq. 20, it can be written as follows.

$$\chi_1(\omega)=\frac{1}{\pi}P\int_{-\infty}^{\infty}\frac{(\Omega+\omega)\chi_2(\Omega)}{(\Omega+\omega)(\Omega-\omega)}d\Omega \quad (22)$$

$$\chi_1(\omega)=\frac{1}{\pi}P\int_{-\infty}^{\infty}\frac{(\Omega+\omega).\chi_2(\Omega)}{\Omega^2-\omega^2}d\Omega \quad (23)$$

$$\chi_1(\omega)=$$
$$=\frac{1}{\pi}P\int_{-\infty}^{\infty}\frac{\Omega\chi_2(\Omega)}{\Omega^2-\omega^2}d\Omega+\frac{1}{\pi}P\int_{-\infty}^{\infty}\frac{\omega\chi_2(\Omega)}{\Omega^2-\omega^2}d\Omega \quad (24)$$

To our aim, if $\chi_2(\Omega)$ is accepted as an odd function ($-\chi_2(\Omega)=\chi_2(-\Omega)$), the second integral in Eq. 24 will be 0 and so Eq. 24 will be written as

$$\chi_1(\omega)=\frac{1}{\pi}P\int_{-\infty}^{\infty}\frac{\Omega\chi_2(\Omega)}{\Omega^2-\omega^2}d\Omega \quad (25)$$

$$\chi_1(\omega)=\frac{2}{\pi}P\int_{0}^{\infty}\frac{\Omega\chi_2(\Omega)}{\Omega^2-\omega^2}d\Omega \quad (26)$$

Relation between complex susceptibility (χ) and complex refractive index (η) is described in Eq. 27.

$$\eta(\omega)=\left(1+\chi(\omega)\right)^{\frac{1}{2}} \quad (27)$$

If Eq. 27 is expanded to Taylor series about 0 (it is known as Maclaurin series) considering $|\chi(\omega)|<1$, Eq. 27 becomes

$$\eta(\omega)\cong 1+\frac{1}{2}\chi(\omega) \quad (28)$$

Complex refractive index is

$$\eta(\omega)\cong n(\omega)+i\kappa(\omega) \quad (29)$$

At Eq. 29, imaginary part of refractive index of an optical material is known as extinction coefficient (κ). If Eq. 15 and Eq. 29 are used in Eq. 28, it becomes

$$n(\omega)+i\kappa(\omega)\cong 1+\frac{1}{2}\left(\chi_1(\omega)+i\chi_2(\omega)\right) \quad (30)$$

Thus,

$$n(\omega) \cong 1 + \frac{1}{2}\chi_1(\omega) \quad (31)$$

$$\kappa(\omega) \cong \frac{1}{2}\chi_2(\omega) \quad (32)$$

If Eq. 31 and Eq. 32 are used in Eq. 26, it becomes

$$2(n(\omega) - 1) = \frac{2}{\pi} P \int_0^\infty \frac{\Omega 2\kappa(\Omega)}{\Omega^2 - \omega^2} d\Omega \quad (33)$$

$$n(\omega) = 1 + \frac{2}{\pi} P \int_0^\infty \frac{\Omega \kappa(\Omega)}{\Omega^2 - \omega^2} d\Omega \quad (34)$$

Where $n(\omega)$ is angular frequency dependent refractive index and $\kappa(\omega)$ angular frequency dependent extinction coefficient. Eq. 34 means that refractive index (that is to say, real part of refractive index) can be calculated from extinction coefficient (that is to say, imaginary part of refractive index). Extinction coefficient of an optical material closely depends on absorption coefficient of that material. The extinction coefficient is given by Eq. 35.

$$\kappa(\Omega) = \frac{\alpha(\Omega)c}{2\Omega} \quad (35)$$

Where $\alpha(\Omega)$ is angular frequency dependent absorption coefficient, c is the speed of light in vacuum and Ω is angular frequency. If Eq. 35 is substituted in Eq. 34, Eq. 34 will be

$$n(\omega) = 1 + \frac{c}{\pi} P \int_0^\infty \frac{\alpha(\Omega)}{\Omega^2 - \omega^2} d\Omega \quad (36)$$

$\alpha(\omega)$ is related with $n(\omega)$ by means of Eq. 36. Refractive index is formulated in terms of the absorption coefficient. Thus, Eq. 36 can be used to calculate refractive index of a given material from its absorption coefficient. Eq. 36 can also be expressed as in Eq. 37.

$$\Delta n = n(\omega) - 1 = \frac{c}{\pi} P \int_0^\infty \frac{\alpha(\Omega)}{\Omega^2 - \omega^2} d\Omega \quad (37)$$

Eq. 36 can be written in terms of wavelength (λ) by using Eq. 38 and Eq. 39.

$$\Omega = \frac{2\pi c}{\lambda'} \quad (38)$$

$$d\Omega = -\frac{2\pi c}{\lambda'^2} d\lambda' \quad (39)$$

Thus, Eq. 36 will be

$$n(\lambda) = 1 + \frac{c}{\pi} P \int_\infty^0 \frac{\alpha(\lambda')}{\left(\frac{2\pi c}{\lambda'}\right)^2 - \left(\frac{2\pi c}{\lambda}\right)^2} \left(-\frac{2\pi c}{\lambda'^2} d\lambda'\right) \quad (40)$$

$$n(\lambda) = 1 + \frac{c}{\pi} P \int_0^\infty \frac{\alpha(\lambda')}{\left(\frac{2\pi c}{\lambda'}\right)^2 - \left(\frac{2\pi c}{\lambda}\right)^2} \left(\frac{2\pi c}{\lambda'^2} d\lambda'\right) \quad (41)$$

$$n(\lambda) = 1 + \frac{1}{2\pi^2} P \int_0^\infty \frac{\alpha(\lambda')}{1 - \left(\frac{\lambda'}{\lambda}\right)^2} d\lambda' \quad (42)$$

Therefore, change in refractive index dependent on wavelength is found as in Eq. 43.

$$\Delta n(\lambda) = n(\lambda) - 1 = \frac{1}{2\pi^2} P \int_0^\infty \frac{\alpha(\lambda')}{1 - \left(\frac{\lambda'}{\lambda}\right)^2} d\lambda' \quad (43)$$

Numerical Computation Method

Trapezoidal rule will be used for evaluation of the integral in Eq. 43 for both equal and unequal steps [16].

Numerical Computation for Equal Wavelength Steps

When measuring the optical transmission spectrum of a material via a monochromator or a spectrophotometer, equal steps can be realized for the wavelength increment. If $\alpha(\lambda)$ is assumed 0 (sufficiently small) outside of the wavelength range λ_1-λ_2, Eq. 43 is written as in Eq. 44 for equal wavelength steps $\Delta\lambda'$.

$$\Delta n(\lambda_u) = \frac{1}{2\pi^2} \sum_{v=1}^{N-1} \frac{1}{2} \left[\frac{\alpha_{v+1}}{1 - \left(\frac{\lambda_{v+1}}{\lambda_u}\right)^2} + \frac{\alpha_v}{1 - \left(\frac{\lambda_v}{\lambda_u}\right)^2} \right] \Delta\lambda' \quad (44)$$

Where N is the number of elements in the array of λ (called as size of the array), and u and v show position numbers in the array of λ (called as its index). For m equal steps from λ_1 to λ_2, $\Delta\lambda'$ is

$$\Delta\lambda' = \frac{\lambda_2 - \lambda_1}{m} \quad (45)$$

If Eq. 45 is substituted in Eq. 44, Eq. 44 will be as follows.

$$\Delta n(\lambda_u) = \frac{1}{2\pi^2}\left(\frac{\lambda_2-\lambda_1}{m}\right)\sum_{v=1}^{N-1}\frac{1}{2}\left[\frac{\alpha_{v+1}}{1-\left(\frac{\lambda_{v+1}}{\lambda_u}\right)^2}+\frac{\alpha_v}{1-\left(\frac{\lambda_v}{\lambda_u}\right)^2}\right] \quad (46)$$

Numerical Computation for Unequal Wavelength Steps

Eq. 43 can be written as in Eq. 47 by using Trapezoidal rule for unequal steps.

$$\Delta n(\lambda_u) = \frac{1}{2\pi^2}\sum_{v=1}^{N-1}\frac{1}{2}\left[\frac{\alpha_{v+1}}{1-\left(\frac{\lambda_{v+1}}{\lambda_u}\right)^2}+\frac{\alpha_v}{1-\left(\frac{\lambda_v}{\lambda_u}\right)^2}\right](\lambda_{v+1}-\lambda_v) \quad (47)$$

Where N is the number of elements in the array of λ (called as size of the array), and u and v show position numbers in the array of λ (called as its index). As understood from Eq. 47, $(\lambda_{v+1}-\lambda_v)$ difference can change during the summation.

An Algorithm for Computation of Refractive Index Change and Refractive Index via Kramers-Kronig Transformation

In Fig. 2, an algorithm to compute refractive index and its change given by Eq. 47 is shown. According to this algorithm, first absorption coefficient measured at each wavelength $(\lambda, \alpha(\lambda))$ has been entered. Then, midpoints (λ_u) between measured successive wavelengths have been calculated. At each λ_u, summation in Eq. 47 has been evaluated for all measured wavelengths (λ_v). Any overlapping between λ_u and λ_v or between λ_u and λ_{v+1} has been prevented by using this approach. Refractive index change (Δn) calculated at each λ_u is saved, and thus refractive index change can be plotted against wavelength. In this algorithm, n_0 can be thought as an offset value and it can take values different from 1. Refractive index is computed by Eq. 48. Weight coefficients w_a and w_b can also be changed around 0.5.

$$n(\lambda_u) = n_0 + \Delta n(\lambda_u) \quad (48)$$

Testing of Computation of Refractive Index

Barium fluoride (BaF_2) crystal has been chosen to try this computation. According to the classical dispersion theory, real and imaginary dielectric constants of BaF_2 are described with following Eqs. 49 and 50 [17, 18]. In Eqs. 49 and 50, λ is in unit of centimeters.

$$\epsilon_1(\lambda) = 2.16 + 152352\frac{33856-\left(\frac{1}{\lambda}\right)^2}{\left(33856-\left(\frac{1}{\lambda}\right)^2\right)^2+13.5424\left(\frac{1}{\lambda}\right)^2}+ +5409.88\frac{77284-\left(\frac{1}{\lambda}\right)^2}{\left(77284-\left(\frac{1}{\lambda}\right)^2\right)^2+6955.56\left(\frac{1}{\lambda}\right)^2} \quad (49)$$

$$\epsilon_2(\lambda) = \frac{560655.36\left(\frac{1}{\lambda}\right)}{\left(33856-\left(\frac{1}{\lambda}\right)^2\right)^2+13.5424\left(\frac{1}{\lambda}\right)^2}+ +\frac{451183.992}{\left(77284-\left(\frac{1}{\lambda}\right)^2\right)^2+6955.56\left(\frac{1}{\lambda}\right)^2} \quad (50)$$

Thus, refractive index, extinction coefficient and absorption coefficient can be found by using Eq. 51, Eq. 52 and Eq. 53, respectively.

$$n(\lambda) = \sqrt{\frac{1}{2}\left(\sqrt{\epsilon_1^2+\epsilon_2^2}+\epsilon_1\right)} \quad (51)$$

$$\kappa(\lambda) = \sqrt{\frac{1}{2}\left(\sqrt{\epsilon_1^2+\epsilon_2^2}-\epsilon_1\right)} \quad (52)$$

$$\alpha(\lambda) = \frac{4\pi}{\lambda}\kappa(\lambda) \quad (53)$$

In Fig. 3b, refractive index of BaF_2 has been plotted by using classical dispersion theory. Then, refractive index of BaF_2 has been derived from α via the numerical K-K transform and it has been plotted over that of the classical dispersion theory. As understood from Fig. 3b, refractive index of BaF_2 has been successfully produced by using this numerical K-K transformation. Similar comparison has been shown for bulk CdSe in Fig. 4.

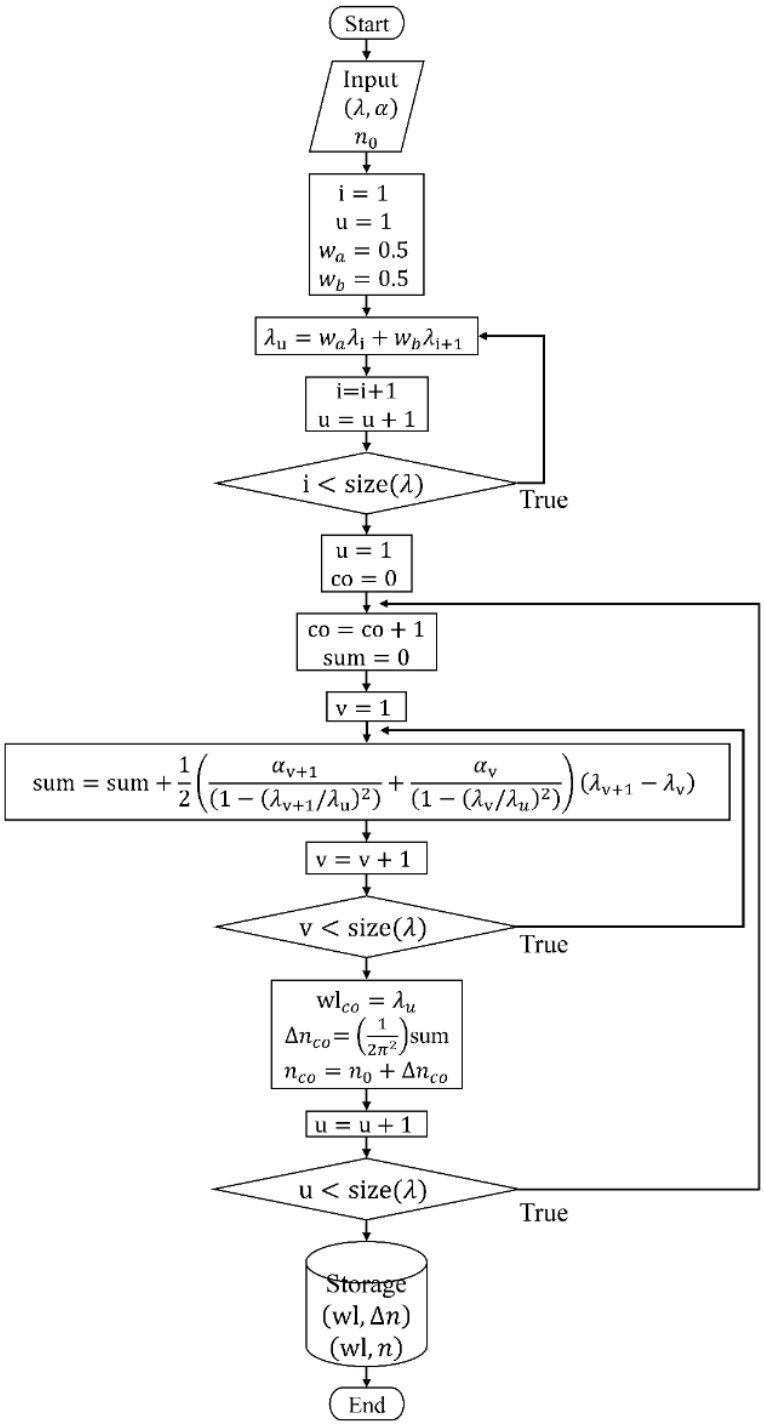

Figure 2 – Flowchart of computation of the refractive index change.

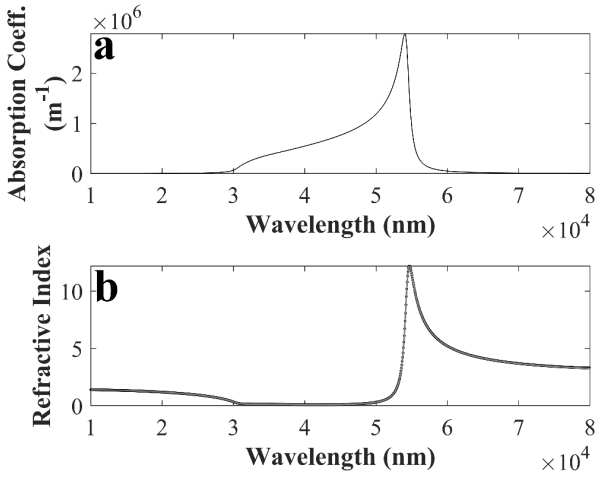

Figure 3 – Absorption coefficient (a) and refractive index (b) of bulk BaF_2. At (b), gray line and black dots correspond to refractive index produced from the classical dispersion theory and K-K transformation, respectively.

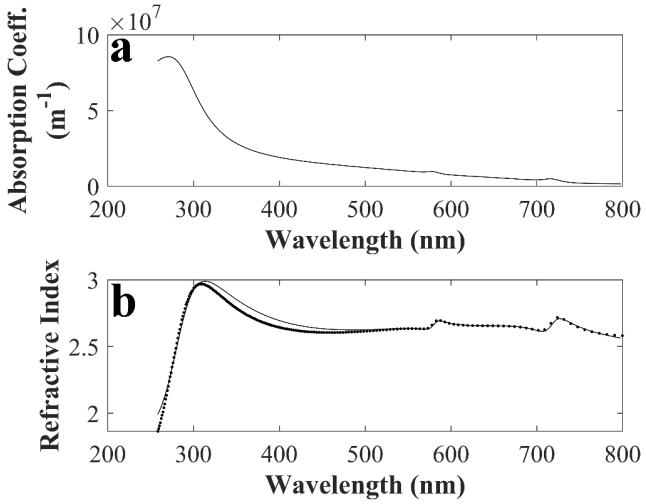

Figure 4 – Absorption coefficient (a) and refractive index (b) of bulk CdSe. At (b), line and dots correspond to refractive index produced from the study of Ninomiya and Adachi [19], and K-K transformation, respectively.

Materials and Methods

Nucleation and Growth Procedure of Small Cadmium Selenide Nanocrystals in Glass

CdSe nanocrystals were nucleated and growth in borosilicate glass. Schott RG695 longpass glass filter was purchased from the Schott company [20]. It was cut into small pieces by a home-made glass cutting machine with a diamond cutting disc. The shapes of these samples were rectangular parallelepiped, and their dimensions were 10 mm, 10 mm, and 2 mm. These glass pieces were melted at 1100°C for 20 min and cooled to room temperature rapidly. Then, samples were put in an alumina boat, loaded into a tube furnace and heat treated at 531°C between 15-75 days in the tube furnace. This temperature corresponds to the glass transition temperature of RG695. After the heat treatment, both surface of each sample was sanded and polished in company with water. Sample thickness was reduced to about 0.430 mm for further optical characterizations.

Optical Characterization of Small Cadmium Selenide Nanocrystals in Glass

Optical absorption and Raman spectra of the samples were measured by home-made optical setups [21]. The Beer-Lambert law was used to compute optical absorption coefficients of the samples

between 430 nm and 900 nm. Samples were excited with 458 nm wavelength laser at Raman measurement.

Results and Discussion

In Fig. 5, optical absorption spectra of CdSe quantum dots in borosilicate glass are shown. sA, sB, sC, sD and sE indicate melted sample, 15 days, 46 days, and 75 days heat treated samples and as received (neither melted nor heat treated) sample, respectively. Absorption of sA is featureless and below ~106 m^{-1} between 430-900 nm. As sA is heat treated, its absorption has begun to evolve. Absorption has increased dramatically at lower wavelengths for sB, however it is featureless again. The first exciton peak has been observed for sC and sD. It shows that CdSe nanocrystals have been grown in glass at the end of 46 days and 75 days. Here, temperature has been lowered, and time interval has been seriously prolonged to produce CdSe nanocrystals in glass differently from those of the studies in literature [6-8]. A shoulder has been seen at that of as received.

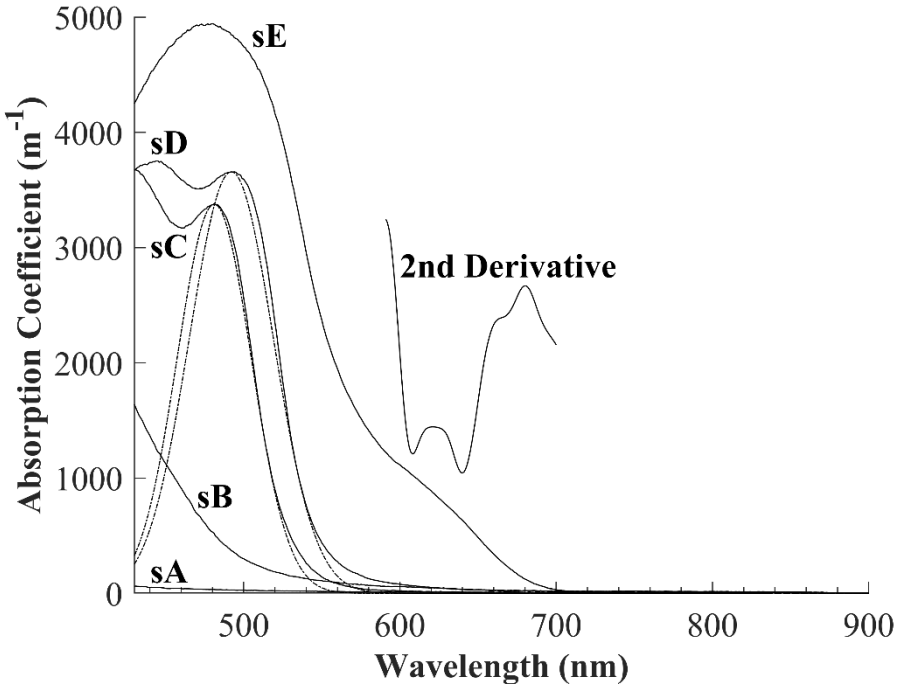

Figure 5 – Optical absorption spectra of CdSe nanocrystals in glass. Sampels; sA: melted, sB: 531°C-15 days, sC: 531°C-46 days, sD: 531°C-75 days, and sE: as received. Dash-dotted lines show Gaussian curves for sC and sD. Second derivative of absorption of sE is indicated.

Average diameter of CdSe quantum dots in glass against their first exciton peak wavelength has been plotted in Fig. 6. This relation is obtained by solving Schrödinger equation considering electron and hole kinetic and Coulomb interaction energies [22]. It is given in Eq. 54.

$$E_{1s1s}(D) = E_g + \frac{2\hbar^2\pi^2}{\mu D^2} - 3.572\frac{e^2}{(4\pi\varepsilon_0)\varepsilon D} \qquad (54)$$

Where E_{1s1s} is first exciton peak energy, E_g is band gap of bulk semiconductor, μ is reduced mass of electron and hole pair, ε_0 is vacuum permittivity, ε is semiconductor nanocrystal's dielectric constant and D is diameter or size of nanocrystal. As seen from Fig. 6, average CdSe nanocrystal size in glass has been found as ~3.80 nm for sC and ~3.93 nm for sD. As a result of growth in size from sC to sD, the peak has shifted to a longer wavelength in the spectrum (see Fig. 5). This observed phenomenon is known as

the quantum size effect [22]. Average size of CdSe nanocrystals for as received sample can be found from the wavelength position of the shoulder. Second derivative of absorption of as received enables us to determine the shoulder position. Minimum of the second derivative is seen at ~640 nm and it corresponds to nanocrystal size of ~7.20 nm.

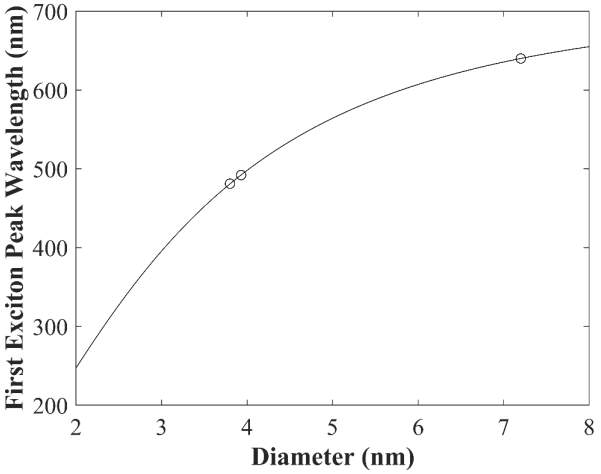

Figure 6 – First peak wavelength versus diameter for CdSe nanocrystals in glass. Circles point out diameters/peak wavelengths for sC, sD and as received. E_g, m_e^*, m_h^* and ε are taken as 1.74 eV, 0.12m$_0$, 0.90m$_0$ and 9.29, respectively. Here, m_e^*, m_h^* and m$_0$ are electron effective mass, hole effective mass and electron rest mass, respectively.

Raman spectrum of sC (indicated with gray color) is shown in Fig. 7. Longitudinal and surface optical (LO and SO) phonon bands of CdSe nanocrystals have been observed. Curve fitting of the spectrum has been made by using Gaussian-Lorentzian curves. LO and 2LO phonon modes have been found about 203 cm^{-1} and 403 cm^{-1}, respectively, and SO phonon mode is at about 182 cm^{-1}. These values are compatible with those of the literature [23, 24]. It has not been encountered with different phonon modes such as CdS-like phonons at Raman measurements of the samples. This observation shows that pure and small CdSe nanocrystals have been created in glass by means of this slow growth process.

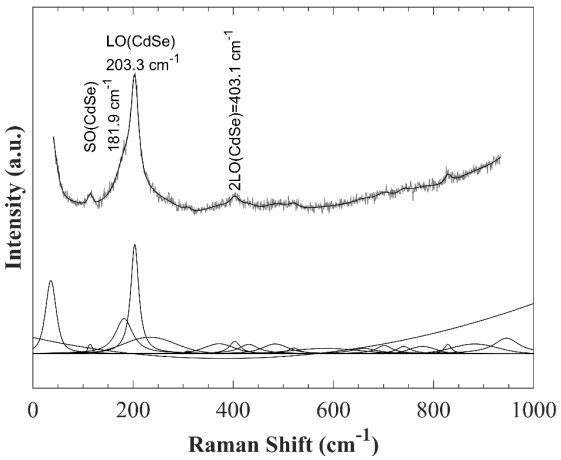

Figure 7 – Raman spectrum of sC. Raman peak positions corresponding to LO and SO phonon modes of CdSe nanocrystals are indicated.

Refractive index changes of the samples have been computed by the K-K transformation and they are shown in Fig. 8. Maximum of refractive index change is at the order of 10^{-7}-10^{-6} for sA. It increases and shifts to longer wavelength with the growth of CdSe nanocrystals in glass. Refractive index change reaches about 1.36×10^{-4} for sD. Refractive index change has increased two orders of magnitude from sA to sD. Maximum refractive index changes of sD and sE are nearly same.

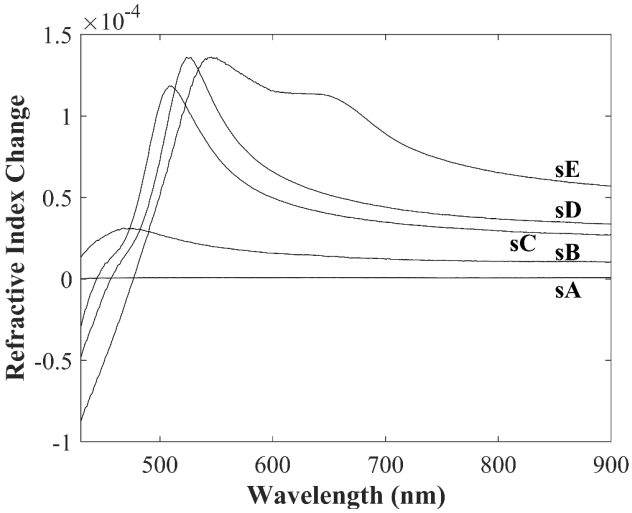

Figure 8 – Refractive index changes of the samples.

Conclusion

CdSe nanocrystals have been successfully grown in borosilicate glass by melting, rapid cooling and heat treatment procedure. Their average diameters have been found to be smaller than the exciton Bohr radius of bulk CdSe, which is around 4.64 nm. Therefore, strong quantum size effect has been obtained and prominent absorption peaks have been appeared at the spectrum of samples of 531ºC-46 hours and 531ºC-75 hours. Raman modes of CdSe nanocrystals having ~3.80 nm have been measured at ~182 cm^{-1} for SO phonons and ~203 cm^{-1} for LO phonons. Refractive index change has been found as high as 1.36×10^{-4} for ~3.93 nm sized CdSe nanocrystals.

Acknowledgments

This study was supported by Toros University (Mersin, Turkey). Equipments of Photonics Laboratory of Physics Department at Yıldız Technical University (Istanbul, Turkey) were used to produce and characterize CdSe nanocrystals in glass. Hence, I would like to thank to Prof.Dr. Hikmet Yükselici (the head of the Photonics Lab.).

References

1. Kronig, R.L. “On the theory of dispersion of X-rays.” *Journal of the Optical Society of America* 12, 6. (1926): 547-557.
2. Kramers, M.H.A. “La diffusion de la lumière par les atomes.” *Atti del Congresso Internazionale dei Fisici*, *Como*. (1927): 545-557.
3. Ganesh, V., Haritha, L., Ali, H.E., Aboraia, A.M., Khairy, Y., Hegazy, H.H., Butova, V., Soldatov, A.V., Algarni, H., Zahran, H.Y., Yahia, I.S. “The detailed calculations of optical properties of indium-doped CdO nanostructured films using Kramers-Kronig relations.” *Journal of Non-Crystalline Solids* 552. (2021): 1-9.
4. Sai, T., Saba, M., Dufresne, E.R., Steiner, U., Wilts, B.D. “Designing refractive index fluids using the Kramers-Kronig relations.” *Faraday Discussions* 223. (2020): 136-144.
5. Hutchings, D.C., Sheik-Bahae, M., Hagan, D.J., Van Stryland, E.W. “Kramers-Krönig relations in nonlinear optics.” *Optical and Quantum Electronics* 24. (1992): 1-30.
6. Munishwar, S.R., Pawar, P.P., Janbandhu, S.Y., Gedam, R.S. “Growth of CdSSe quantum dots in borosilicate glass by controlled heat treatment for band gap engineering.” *Optical Materials* 86. (2018): 424-432.
7. Dey, C., Goswami, M., Karmakar, B. “CdSe nanocrystals ingrained dielectric nanocomposites: synthesis and photoluminescence properties.” *Materials Research Express* 2, 1. (2015): 1-12.
8. Azhniuk, Y.M., Gomonnai, A.V., Hutych, Yu.I., Lopushansky, V.V., Zahn, D.R.T. “Optical characterization of $CdSe_{1-x}Te_x$ nanocrystals grown in borosilicate glass.” *Journal of Nano- and Electronic Physics* 14, 4. (2022): 1-6.
9. Moreels, I., Allan, G., Geyter, B.D., Wirtz, L., Delerue, C., Hens, Z. “Dielectric function of colloidal lead chalcogenide quantum dots obtained by a Kramers-Krönig analysis of the absorbance spectrum.” *Physical Review B* 81, 23. (2010): 1-7.
10. Moreels, I., Kruschke, D., Glas, P., Tomm, J.W. “The dielectric function of PbS quantum dots in a glass matrix.” *Optical Materials Express* 2, 5. (2012): 496-500.
11. Dement, D.B., Puri, M., Ferry, V.E. “Determining the complex refractive index of neat CdSe/CdS quantum dot films.” *Journal of Physical Chemistry C* 122, 37. (2018): 21557-21568.
12. Nguyen, T.T., Tran, V.T., Seok, J.S., Lee, J.H., Ju, H. “Quantum dot-induced blue shift of surface plasmon spectroscopy.” *Nanomaterials* 12, 12. (2022): 1-10.
13. Garcia, H., Serna, J., Rueda, E. “Bulk ZnSe and CdS two-photon absorption measurement with an F-scan nonlinear absorption spectrometer.” *OSA Continuum* 3, 3. (2020): 498-504.
14. Nootz, G., Padilha, L.A., Webster, S., Hagan, D.J., Van Stryland E.W. “Resonant nonlinear optical properties of CdSe quantum dots.” *Conference on Lasers and Electro-Optics, Baltimore, United States*. (2007). CThV2.
15. Islamov, Y., Amirov, Z. “A(z)-application of ananlytic function Jordan’s lemma.” *Texas Journal of Multidisciplinary Studies* 4. (2022): 194-197.
16. Abdulhameed, A.F., Memon, Q.A. “An improved trapezoidal rule for numerical integration.” *Journal of Physics: Conference Series*, *10th International Conference on Mathematical Modeling in Physical Sciences* 2090. (2021): 1-9.
17. Kaiser, W., Spitzer, W.G., Kaiser, R.H., Howarth, L.E. “Infrared properties of CaF_2, SrF_2, and BaF_2.” *Physical Review* 127, 6. (1962): 1950-1954.
18. Kelly-Gorham, M.R.K., DeVetter, B.M., Brauer, C.S., Cannon, B.D., Burton, S.D., Bliss, M., Johnson, T.J., Myers, T.L. “Complex refractive index measurements for BaF_2 and CaF_2 via single-angle infrared reflectance spectroscopy.” *Optical Materials* 72. (2017): 743-748.

19. Ninomiya, S., Adachi, S. “Optical properties of cubic and hexagonal CdSe.” *Journal of Applied Physics* 78, 7. (1995): 4681-4689.

20. Schott. RG695. https://www.schott.com/shop/advanced-optics/en/Matt-Filter-Plates/RG695/c/glass-RG695. (accessed February 20, 2023).

21. Yükselici, M.H., Bozkurt, A.A., Ömür, B.C. “A detailed examination of the growth of CdSe thin films through structural and optical characterization.” *Materials Research Bulletin* 48, 7. (2013): 2442-2449.

22. Efros, A.L., Brus, L.E. “Nanocrystal quantum dots: from discovery to modern development.” *ACS Nano* 15, 4. (2021): 6192-6210.

23. Azhniuk, Y.M., Gomonnai, A.V., Hutych, Y.I., Lopushansky, V.V., Prots, L.A., Turok, I.I., Zahn, D.R.T. “Evidence for formation of Se molecular clusters during precipitation of $CdSe_{1-x}S_x$ nanoparticles in glass.” *Applied Physics A* 95. (2009): 473-477.

24. Singha, A., Roy, A. “Phonon confinement and surface phonon modes in CdSe-CdS core-shell nanocrystals.” *Reviews on Advanced Materials Science* 10, 5. (2005): 462-466.